Transforming the Dynamic Response of Robotic Structures and Systems Through Laminar Jamming

Yashraj S. Narang , Alperen Degirmenci , Joost J. Vlassak, and Robert D. Howe

Abstract—Researchers have developed variable-impedance mechanisms to control the dynamic response of robotic systems and improve their adaptivity, robustness, and efficiency. However, these mechanisms have limitations in size, cost, and convenience, particularly for variable damping. We demonstrate that laminar jamming structures can transform the dynamic response of robotic structures and systems while overcoming these limitations. In laminar jamming, an external pressure gradient is applied to a laminate of compliant material, changing its stiffness and damping. In this latter, we combine analysis, simulation, and characterization to formulate a lumped-parameter model that captures the nonlinear mechanical behavior of jamming structures and can be used to rapidly simulate their dynamic response. We illustrate that by adjusting the vacuum pressure, the fundamental features of the dynamic response (i.e., frequency, amplitude, decay rate, and steady-state value) can be tuned on command. Finally, we demonstrate that jamming structures can be integrated into soft structures and traditional rigid robots to considerably alter their response to impacts. With the models and demonstrations provided here, researchers may move further toward building versatile and transformative robots.

Index Terms—Soft material robotics, compliant joint/ mechanism, dynamics, compliance and impedance control, aerial systems: mechanics and control.

I. INTRODUCTION

THE dynamic response of a robotic system is one of its most fundamental properties. It is defined as the transient and steady-state behavior of an output in response to a time-varying input (e.g., the oscillation in the position of a robotic arm after an impulse of force). When a robotic system interacts with the environment, actively controlling the dynamic response of the system can improve its safety, adaptivity, robustness, and energy efficiency [1].

The leading approach to controlling dynamic response is tuning mechanical impedance (i.e., stiffness and damping); thus, researchers have focused on developing variable-impedance mechanisms [1]–[4]. However, existing mechanisms have

Fig. 1. Vacuum-based implementation of laminar jamming. (A) Layers of compliant material are enclosed in an airtight envelope connected to a vacuum line. (B) When no vacuum is applied, the structure is compliant in bending. When vacuum is applied, the structure is stiff.

notable limitations. In particular, variable-damping mechanisms are predominantly hydraulic (e.g., magneto/electrorheological fluids) or electromagnetic (e.g., Eddy currents); these systems are often large, heavy, expensive, and difficult to manufacture [1].

Researchers have also investigated a variable-impedance mechanism called laminar jamming (a.k.a., "layer jamming"). In laminar jamming, an external pressure gradient is applied to layers of compliant material (e.g., via a vacuum), increasing the initial bending stiffness of the structure by a factor of n^2, where n is the number of layers (Fig. 1). Laminar jamming has been used as a variable-stiffness mechanism in haptics, rehabilitation, medical devices, and soft robots [5]–[12].

As recently described [12], laminar jamming structures may also act as a variable-damping mechanism. When a jammed structure is initially deformed, its layers are cohesive, and its stiffness is maximal. However, when a critical load is applied, its layers begin to slip, and its stiffness decreases; moreover, energy is dissipated to friction between the layers. In this regime, the friction damping (i.e., energy dissipated per unit deflection) increases linearly with the external pressure gradient. In contrast to other variable-damping mechanisms, laminar jamming structures are thin, lightweight, low cost, and simple to fabricate.

The controllable stiffness and damping of jamming structures may be combined to form a variable-impedance mechanism with a tunable dynamic response. Nevertheless, no studies have investigated these capabilities.
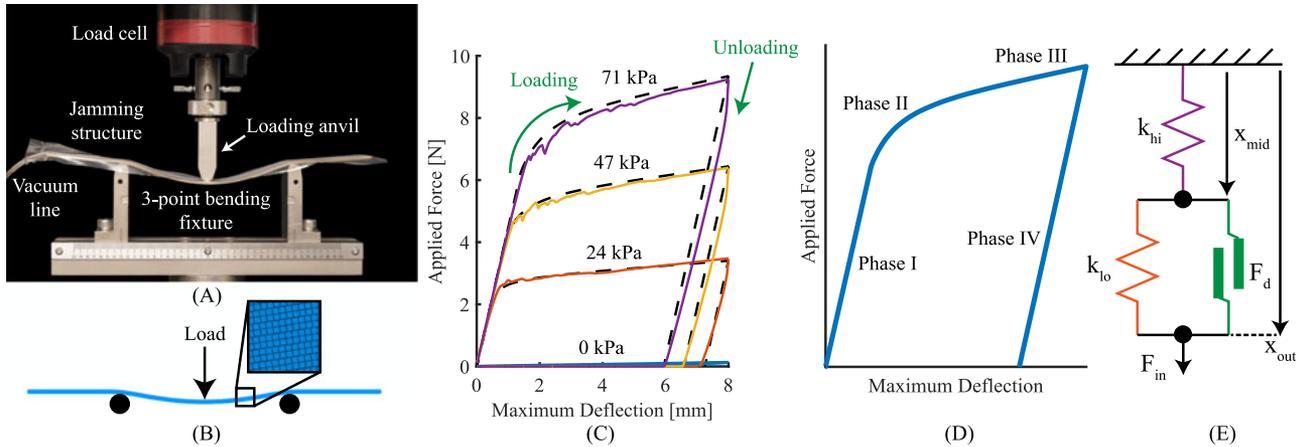
Fig. 2. Quasi-static behavior of laminar jamming structures. (A) Experimental characterization setup. (B) Corresponding finite element model. Inset shows slip between adjacent layers. (C) Experimental (colored) and finite element (dashed) force-deflection curves over one loading cycle at four different vacuum pressures. (D) Fundamental phases of deformation. (E) Schematic of quasi-static lumped-parameter model.

In this study, we demonstrate that laminar jamming can transform the dynamic response of robotic structures and systems. We combine analysis, simulation, and experiments to predict and measure the nonlinear static and dynamic behavior of jamming structures, and we determine that this complex behavior is captured by a lumped-parameter model that can be rapidly simulated. Furthermore, we show that by adjusting the pressure gradient applied to a jamming structure, the fundamental features of its dynamic response (i.e., frequency, amplitude, and steady-state deformation) can be considerably altered. We then integrate laminar jamming structures into soft structures and unmanned aerial vehicles (UAVs) to illustrate that by adjusting the dynamic response of jamming structures, the impact response of both soft and traditional rigid robots can be transformed as well.

Thus, we demonstrate that laminar jamming is a useful variable-impedance mechanism that resolves several drawbacks of existing variable dampers. Furthermore, we provide designers with an analytical toolkit for building jamming structures to meet specific dynamic requirements.

II. METHODS AND RESULTS

A. Development of Lumped-Parameter Models

In this section, we develop a method to rapidly predict how laminar jamming structures deform under static and dynamic loads. To do so, we measure quasi-static force-deflection curves of jamming structures and predict them using finite element simulations. However, these simulations can be difficult to generalize and require days to complete. Thus, we subsequently formulate a quasi-static lumped-parameter model that provides intuition and can execute in seconds. We calibrate the model and show that it can predict experimental force-deflection curves. Finally, we formulate a dynamic lumped-parameter model and predict dynamic responses, which are validated in the next section.

1) Quasi-Static Experimental Characterization: Prior to experimental characterization, a jamming structure was fabricated.

The structure consisted of twenty 250 mm × 50 mm layers of copy paper enclosed in an airtight envelope made of 0.076 mm-thick thermoplastic elastomer film (Stretchlon 200, Fibre Glast Developments Corp., Brookville, OH). The structure was then characterized on a materials testing machine (Instron 5566, Illinois Tool Works, Norwood, MA) in three-point bending (Fig. 2(A)). The structure was centered on a bending fixture with the supporting anvils placed 130 mm apart and connected to a vacuum regulator set to the desired vacuum pressure (defined as the pressure inside the envelope below ambient pressure). A loading anvil attached to a 100 N load cell was lowered until contacting the structure. Force and displacement data were then recorded as the anvil was lowered by 8 mm and returned to its original position at $25 \frac{\text{mm}}{\text{s}}$.

The laminar jamming structure was tested at four different vacuum pressures, with three trials per pressure. For each vacuum pressure, mean force-displacement curves were computed. The results are shown in Fig. 2(C).

2) Quasi-Static Finite Element Modeling: Laminar jamming structures were modeled using finite element software (ABAQUS v6.14r2, Dassault Systemes, Villacoublay, France) according to a procedure first described in recent work [12]. Each layer was modeled as a 2D plane-strain structure with dimensions equal to their experimental dimensions. The elastic modulus E and static coefficient of friction μ were equal to measured values ($E = 6$ GPa, $\mu = 0.65$), and the Poisson's ratio ν was equal to the literature value ($\nu = 0.156$)[13]. At the interfaces between layers, frictional contact was prescribed. Large-deformation analysis was enabled.

The structure was constrained in three-point bending, and pressure (equal to the vacuum pressure) was applied to the outer edges. A linearly increasing force was applied to the center of the top layer over 200 equal increments until a deflection of 8 mm (Fig. 2(B)). The load was then linearly decreased to zero over 200 equal increments. Simulation results are shown in Fig. 2(C). Note that no simulation results are provided for a vacuum pressure of 0 kPa, as the model was unstable without pressure.
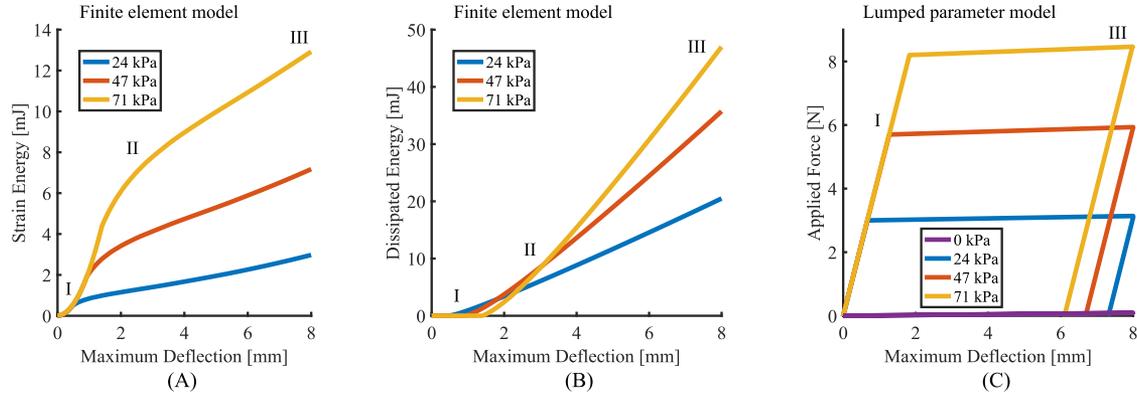
Fig. 3. Calibration and simulation of quasi-static lumped-parameter model. (A) Finite element results for strain energy versus maximum deflection. (B) Finite element results for dissipated energy versus maximum deflection. (C) Quasi-static simulations of lumped-parameter model in three-point bending.

Finite element results agreed closely with experimental results, demonstrating that the behavior of jamming structures can be accurately predicted using finite element simulations. Furthermore, the results showed that the force-deflection curves at all nonzero vacuum pressures exhibited classical hysteresis loops. The energy dissipated per unit cycle (i.e., area under the hysteresis curves) and friction damping (i.e., energy dissipated per unit deflection) scaled linearly with vacuum pressure, indicating that damping can be controlled by simply adjusting vacuum pressure.

Each hysteresis loop consisted of four distinct phases (Fig. 2(D)). In Phase I, the bending stiffness (proportional to the slope of the curve) was maximal and constant. In Phase II, the stiffness gradually decreased. In Phase III, the stiffness was minimal and approximately constant. Finally, in Phase IV, the structure was unloaded, and the slope of the curve matched that of Phase I. From the finite element simulations, it was found that in Phases I and IV, no slip occurred at the interfaces between the layers, and no energy was dissipated. In Phase II, slip occurred at increasingly long sections of the interfaces, and in Phase III, slip occurred at all possible sections of the interfaces; in both Phase II and Phase III, energy was dissipated to friction.

3) Quasi-Static Lumped-Parameter Model: The lumped-parameter model consisted of a stiff spring with stiffness k_{hi} in series with a parallel unit, which itself consisted of a compliant spring with stiffness k_{lo} (where $k_{lo} << k_{hi}$) and friction damper with damping force F_d (Fig. 2(E)). The springs had an equilibrium length of zero. Force F_{in} modeled the transverse force applied to the jamming structure, and deflection x_{out} modeled the maximum deflection.

When F_{in} is small, the damper is rigid, and the compliant spring cannot deform. Thus, k_{hi} governs the stiffness of the system. This phase of deformation corresponds to Phase I. As F_{in} increases, the force on the damper exceeds F_d. The damper is no longer rigid, and the compliant spring can deform. Because $k_{lo} << k_{hi}$, quantity k_{lo} governs the stiffness of the system. This phase corresponds to Phase III. Finally, when F_{in} is decreased, the damper is once again rigid, and k_{hi} governs the stiffness of the system. This phase corresponds to Phase IV. Note that Phase II is not modeled.

Before the lumped-parameter model could be simulated, its coefficients needed to be calibrated. Finite element results were

TABLE I
COEFFICIENTS OF LUMPED-PARAMETER MODEL (3-POINT BENDING)

Pressure	Coefficient			
[kPa]	$k_{hi}[\frac{N}{mm}]$	$k_{lo}[\frac{N}{mm}]$	$F_d[N]$	$m_{eff}(g)$
0	N/A	0.0112	0	5.4
24	4.48	0.0192	2.99	5.4
47	4.46	0.0345	5.71	5.4
71	4.46	0.0432	8.24	5.4

chosen as reference data; however, experimental data could have been used as well.

Energetic equivalence was prescribed between the finite element model and the lumped-parameter model. Strain energy E_s and dissipated energy E_d were extracted from the finite element model over Phases I–III and plotted versus deflection (Fig. 3(A) and (B)). For the lumped-parameter model, analytical expressions for dissipated energy and strain energy can be derived. For positive F_{in}, these energies are

$$E_s = \frac{1}{2}(k_{hi}x_{mid}^2 + k_{lo}(x_{out} - x_{mid})^2), \qquad (1)$$

$$E_d = F_d(x_{out} - x_{mid}). \qquad (2)$$

During Phase I, $x_{out} = x_{mid}$, as the springs have an initial length of zero and only the stiff spring can deform. Furthermore, during Phase III, x_{mid} is approximately constant, as $k_{lo} << k_{hi}$ and the additional deformation of the stiff spring is negligible. Thus, during Phase I,

$$k_{hi} = \frac{\partial^2 E_s}{\partial x_{out}^2}. \qquad (3)$$

During Phase III,

$$k_{lo} = \frac{\partial^2 E_s}{\partial x_{out}^2}, \qquad (4)$$

$$F_d = \frac{\partial E_d}{\partial x_{out}}. \qquad (5)$$

Given energetic equivalence, these formulae were applied to finite element results to determine k_{hi}, k_{lo}, and F_d at each vacuum pressure. The results are aggregated in Table I. Note that k_{hi} was identical for all nonzero pressures. At 0 kPa, no friction
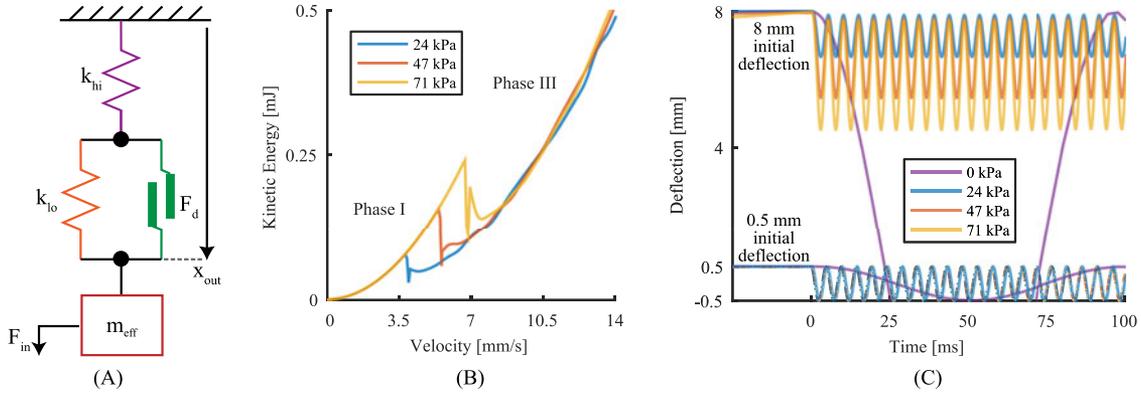
Fig. 4. Calibration and simulation of dynamic lumped-parameter model. (A) Schematic of dynamic lumped-parameter model. (B) Finite element results for kinetic energy versus velocity at the point of maximum deflection. (C) Simulated step responses of lumped-parameter model.

is present; thus, $k_{hi} = F_d = 0$. Since no finite element simulations were conducted at 0 kPa, k_{lo} was calculated using the previously described analytical result that the bending stiffness of a jamming structure without vacuum is equal to its initial stiffness with vacuum, divided by n^2 [5], [12], [14].

The lumped-parameter model was then simulated using dynamic simulation software (SimScape 2016b, The MathWorks, Inc., Natick, MA). The simulations executed in seconds on a laptop computer. The results are shown in Fig. 3(C). As desired, lumped-parameter results closely matched experimental and finite element data (Fig. 2(C)). Of course, Phase II was not replicated; however, designers can still use the model to rapidly predict stiffness and energy dissipation for both small and large loads.

4) Dynamic Lumped-Parameter Model: Although the preceding lumped-parameter model accurately predicted the quasi-static behavior of jamming structures, it could not simulate the dynamic response (e.g., step response). Since the dominant damping phenomenon in laminar jamming structures is dry friction, which is velocity-independent, it was hypothesized that to simulate dynamics, only an additional effective mass was needed (Fig. 4(A)).

To calibrate the magnitude m_{eff} of the effective mass, a dynamic-implicit finite element simulation was executed. The simulation had identical parameters to the quasi-static simulation; in addition, the mass density of the layers was equal to the experimental value (i.e., 7.75e3 $\frac{\text{kg}}{\text{m}^3}$).

Energetic equivalence was again prescribed between the finite element model and the lumped-parameter model. Kinetic energy was extracted from the finite element results, plotted versus velocity at the point of maximum deflection, and low-pass filtered with cutoff frequency 3 Hz (Fig. 4(B)). As before, no simulation results are provided for 0 kPa, as the model was unstable without pressure. The kinetic energy exhibited an anticipated transient dropoff and numerical noise when Phase I ended and energy dissipation commenced. The kinetic energy of the lumped-parameter model is

$$E_k = \frac{1}{2} m_{\text{eff}} v_{\text{out}}^2 \qquad (6)$$

where v_{out} is velocity at $x = x_{\text{out}}$. Thus,

$$m_{\text{eff}} = \frac{\partial^2 E_k}{\partial v_{\text{out}}^2}. \qquad (7)$$

Quantity m_{eff} was identical during Phase I and Phase III and constant at all pressures (Table I). (Since no finite element simulations were conducted at 0 kPa, m_{eff} was assigned to the value at the nonzero pressures.) This result was expected, as the jamming structure experienced small displacements; thus, the geometry (and in turn, the mass distribution) of the structure does not change significantly between phases or pressures. Note that m_{eff} is nearly identical to the value calculated from the well-known formula for the effective mass of a simply-supported beam (i.e., $m_{\text{eff}} = 0.5\,m$) [15]. Thus, in subsequent simulations, effective-mass formulae can be used.

A step response was then simulated. The model was initially displaced to deflections of 0.5 mm and 8 mm, and F_{in} was then released. Fig. 4(C) shows the subsequent time responses for x_{out} at each vacuum pressure.

For the 0.5 mm initial deflection, the loads were not large enough at any pressure to deform the damper. As expected, the nonzero-pressure conditions oscillated with equal frequencies, as k_{hi} was effectively identical. However, the zero-pressure condition oscillated with a frequency that was a factor of n lower, as its stiffness was n^2 smaller. The amplitudes in the nonzero- and zero-pressure conditions were all identical, as no energy was dissipated to friction.

For the 8 mm initial deflection, the loads were large enough at all pressures to deform the damper. Identical to the 0.5 mm cases, the nonzero pressure conditions oscillated with equal frequencies, and the zero-pressure condition oscillated with a frequency that was a factor of n lower; furthermore, the zero-pressure condition maintained its initial amplitude, as no energy was dissipated. However, for the nonzero-pressure conditions, as pressure increased, the oscillations had larger amplitudes and a mean value that was closer to initial equilibrium (i.e., 0 mm). These results can be expected; as pressure increases, the ratio of strain energy to dissipated energy after F_{in} is released also increases.
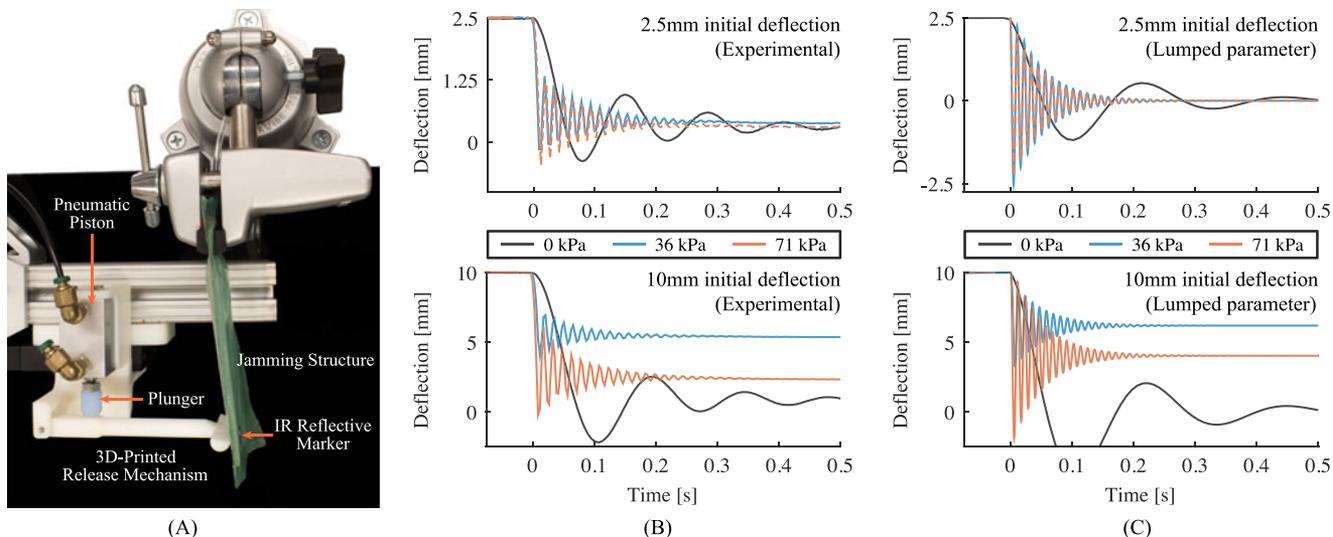
Fig. 5. Characterization and simulation of dynamic response of jamming structures. (A) Experimental setup to measure step response of jamming structure. (B) Experimental step responses at small and large initial deflections, each at multiple vacuum pressures. (C) Corresponding lumped-parameter step responses.

The preceding results indicate that the variable-stiffness behavior of a jamming structure may enable the oscillation frequency to be markedly altered by simply turning vacuum on and off. Furthermore, for large initial deflections, the variable-damping behavior of the structure may allow the amplitude of oscillation and steady-state deformation to be tuned on command by adjusting vacuum pressure.

B. Evaluation of Dynamic Lumped-Parameter Model

In the previous section, we used quasi-static experiments, simulation, and analysis to propose a dynamic lumped-parameter model. In this section, we experimentally evaluate the lumped-parameter model and show that it indeed predicts dynamic responses; thus, designers can use the models to rapidly predict dynamic behavior.

Although quasi-static force-deflection behavior was analyzed in three-point bending, we now examine dynamic responses in cantilever bending. This loading condition is more common in real-world dynamic robots (e.g., manipulators); furthermore, the investigation shows that the analytical methods proposed are agnostic to loading conditions and may be used by designers in diverse physical scenarios.

1) Dynamic Experimental Characterization: The dynamic response of laminar jamming structures was characterized on a custom experimental setup (Fig. 5(A)). A twenty-layer 125 mm × 50 mm jamming structure was fabricated, and a circular fiducial marker was cut from infrared (IR)-reflective fabric (RF-HW25400, Nanning V-Can Business Co., Ltd., Nanning, China) and adhered to the jamming envelope. The position of the marker was measured using an optical tracking system (FusionTrack 500, Atracsys, Switzerland) with an accuracy of 90 μm and sampling rate of 335 Hz.

At the beginning of each test, the jamming structure was connected to a vacuum regulator set to a desired vacuum pressure, and the structure was clamped horizontally. When a pneumatic solenoid was actuated, a plunger pushed a release mechanism

TABLE II
COEFFICIENTS OF LUMPED-PARAMETER MODEL (CANTILEVER)

Pressure	Coefficient			
[kPa]	$k_{hi}\left[\frac{N}{mm}\right]$	$k_{lo}\left[\frac{N}{mm}\right]$	$F_d[N]$	$m_{\text{eff}}(g)$
0	N/A	0.00153	0	2.0
36	0.614	0.0040	2.10	2.0
71	0.614	0.0086	3.71	2.0

that rapidly rotated and released the tip of the jamming structure, implementing a step force input.

Two jamming samples were tested with initial deflections of 2.5 mm and 10 mm at vacuum pressures of 0 kPa, 36 kPa, and 71 kPa. Mean time responses are shown in Fig. 5(B).

2) Dynamic Lumped-Parameter Model: Coefficients of the lumped-parameter model for cantilever bending were extracted using the process described earlier. Energetic equivalence was again prescribed, and (3)–(5) were used to compute the coefficients for the springs and dampers. As validated earlier, effective-mass formulae were used to determine m_{eff} (for a cantilever beam, $m_{\text{eff}} = \frac{33}{140}m$). The coefficients are provided in Table II. The resulting time responses are also shown in Fig. 5(C); note that to model experimentally-observed air drag, the model responses were multiplied by exponential decay functions with empirically determined time constants of 0.14 s for the zero-pressure conditions and 0.05 mnbsps for the nonzero-pressure conditions.

The lumped-parameter model exhibited the same fundamental trends as the experimental data. In both the experimental and lumped-parameter results, for both small and large deflections, the oscillation frequencies of the nonzero-pressure conditions were approximately identical, and the frequencies of the zero-pressure conditions were approximately a factor of n lower. (Experimental frequency reductions were slightly less than n due to imperfect clamping of the jamming structures.) In both the experimental and lumped-parameter results for the large ini-
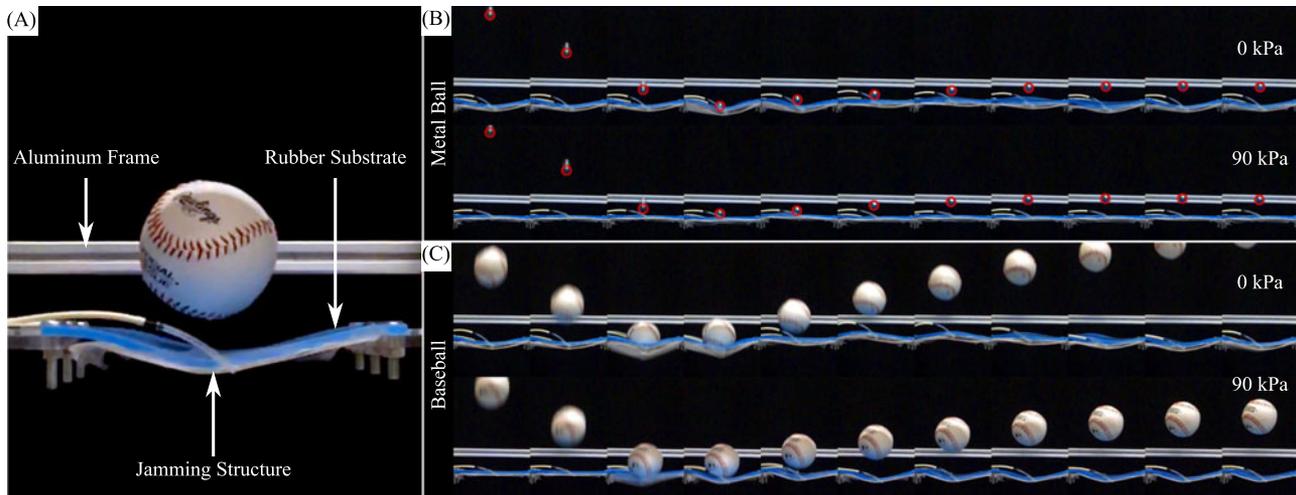
Fig. 6. Tuning the impact response of soft structures using laminar jamming. (A) Experimental setup prior to collision. (B) Representative time series of collision with a metal ball without and with vacuum. Ball is outlined in red. (C) Representative time series of collision with a baseball. (Video S1)

tial deflection, oscillation amplitudes increased with vacuum pressure, and steady-state deformations were closer to initial equilibrium (i.e., 0 mm). These trends are identical to those observed for the model in three-point bending and have the same physical basis.

The lumped-parameter results were also numerically accurate. For both small and large deflections at 0 kPa and 36 kPa, as well as small deflections at 71 kPa, the steady-state deformation value for the lumped-parameter model was within 0.5 mm of the experimental value. However, for large deflections at 71 kPa, the steady-state value for the model ($\approx$4.5 mm) was greater than the experimental value ($\approx$2.5 mm). This discrepancy likely arises from neglecting Phase II in the model, which consequently underestimates the elastic energy stored in the structure prior to release.

To provide additional physical insight, dynamic finite-element simulations of the post-release oscillations were executed, and dissipated energy was extracted. It was found that all energy dissipated to friction was dissipated immediately. In terms of the lumped-parameter model, the friction damper deformed immediately after release; however, once the damper stopped deforming, it never deformed again.

The preceding results demonstrate that lumped-parameter models based on quasi-static cyclic loading tests can accurately predict the dynamic response (e.g., step response) of jamming structures. Furthermore, the experimental and lumped-parameter results offer further evidence that vacuum pressure can dramatically alter dynamic response. By applying vacuum pressure, the variable-stiffness properties of jamming structures can increase the oscillation frequency by approximately a factor of n. Furthermore, by increasing vacuum pressure, the variable-damping properties of the structures can increase the oscillation amplitude and drive steady-state deformation closer to initial equilibrium.

C. Controlling Impacts With Laminar Jamming

In previous sections, we showed that by adjusting the vacuum pressure, the dynamic response of jamming structures can be altered on command. In this section, we demonstrate that by integrating jamming structures into real-world robotic structures and systems, the impact responses of such systems can be transformed as well.

1) Tuning the Impact Response of Soft Structures: A twenty-layer 150 mm $\times$ 150 mm jamming structure was fabricated. To represent a typical soft-robotic structure, a 5 mm-thick substrate of identical area was cast from Shore 50 A silicone rubber (Smooth-Sil 950, Smooth-On, Macungie, PA), a material used in soft actuators. The jamming structure was then adhered to the rubber. The composite structure (i.e., the substrate and jamming structure) was bolted on two sides to an aluminum frame (Fig. 6(A)); slack was introduced to reduce the effect of membrane forces on initial stiffness.

A 25 mm-diameter steel ball (28 g) and a 72 mm-diameter baseball (158 g) were dropped onto the composite structure from a height of 1.5 m with and without vacuum applied to the jamming structure. An alignment fixture was constructed to drop the objects with high positional repeatability. The collisions were filmed at 240 fps using a high-speed video camera. Representative time series are shown in Fig. 6(B) and (C).

Fig. 6(B) illustrates that the metal ball rebounded to similar heights with and without vacuum. These results imply that the impact forces were not large enough to drive the jamming structure from Phase I to Phase II, and that energy was not dissipated in the jamming structure; this conclusion is further supported by the images of the vacuum condition, which show negligible deformation of the composite structure.

On the other hand, Fig. 6(C) illustrates dramatically different dynamic responses for the baseball. The baseball without vacuum repeatedly rebounded to a minimum of three times the height of the baseball with vacuum. These results imply that impact forces were indeed enough to drive the jamming structure into Phase II, and that significant energy was dissipated in the jamming structure; this conclusion is validated by the images of the composite structure after collision, which show transient oscillations without vacuum, but a large permanent deformation with vacuum.

The preceding results demonstrate that jamming structures can effectively tune the impact responses of soft-robotic structures. Without vacuum, the energy of an incoming projectile and the original equilibrium deformation of the target can both be maximally preserved; with vacuum, the energy of the incoming projectile can be sharply dissipated.

2) Tuning the Impact Response of Traditional Rigid Robots: Four twenty-layer 125 mm × 50 mm jamming structures were fabricated. A 3D-printed fixture was designed that cantilevered the jamming structures at 30° from the bottom of a UAV (Syma X5C Quadcopter, Guangdong Syma Model Aircraft Indl Co Ltd, Shantou, China), constituting landing gear (Fig. 7(A)). As in the dynamic experimental characterization, an IR-reflective fiducial marker was mounted on the UAV and tracked using an IR camera at 335 Hz.

The tests were designed to simulate slow and fast landings of a UAV. It was hypothesized that for a given landing velocity, there existed an ideal vacuum pressure for the jamming structures that would simultaneously minimize peak forces on the UAV while also preventing its chassis from bottoming out (i.e., striking the ground).

During each test, the vacuum pressure on all four jamming structures was set to a desired level. The system was then maneuvered to desired landing velocities by adjusting drop height and propeller speed. The resulting collisions were filmed at 60 fps and are illustrated in Fig. 7(B).

On immediate inspection, the results once again demonstrate that by adjusting vacuum pressure on laminar jamming structures, the dynamic response of a robotic system can be transformed. For a given velocity, different pressures showed markedly distinct oscillation amplitudes, frequencies, and decay rates. Furthermore, the results supported our hypothesis; at a given landing velocity, an ideal pressure for the jamming structures did exist. Specifically, it was the minimum pressure that still prevented the chassis from bottoming out. At a landing velocity of 1 m/s, the 0 kPa condition bottomed out and exhibited the highest peak forces (approximated by the second derivative of the displacement-versus-time curve). Among the remaining pressure conditions, the 36 kPa condition was ideal, as it exhibited lower peak forces and a higher decay rate. Given that the initial stiffnesses of the jamming structures in the nonzero-pressure conditions are identical, the higher initial oscillation amplitude in the 36 kPa condition indicates that the structures entered Phase II and dissipated kinetic energy. At a landing velocity of 2 m/s, both the 0 kPa and the 36 kPa conditions bottomed out; however, the 71 kPa condition did not and was thus ideal.

The preceding results demonstrate that jamming structures can also be integrated into traditional rigid robotic systems to rapidly tune impact responses. Furthermore, given their light weight, high damping force range, and effectively infinite damping resolution, jamming structures may constitute a compelling mechanism for active UAV landing gear.

III. DISCUSSION

The present work offers several contributions. First, it demonstrates that laminar jamming structures constitute an effective variable-impedance mechanism that overcomes several limitations of existing mechanisms, particularly variable dampers. As described earlier, by applying vacuum pressure, the stiffness of a jamming structure can be increased by a factor of n^2, where n is the number of layers; furthermore, for large forces (i.e., in Phase III), energy dissipation and friction damping scale linearly with the vacuum pressure. Through experiments and simulations, it was shown that the variable-stiffness properties of jamming structures allow oscillation frequencies to be adjusted, whereas the variable-damping properties enable oscillation amplitudes, decay rates, and steady-state deformations to be tuned on command. Furthermore, these functions are realized in a form that is thin, lightweight, low cost, and easy to manufacture, ameliorating the drawbacks of existing mechanisms.

Second, the paper illustrates that laminar jamming can effectively tune the dynamic responses of real-world robotic structures and systems. Through experimental demonstrations, it was shown that the impact response of soft structures (i.e., soft substrates with integrated jamming structures) can be tuned to conserve or dissipate energy as desired. For an incoming projectile with high kinetic energy, relieving vacuum pressure from the jamming structures allows the energy of the projectile to be maximally preserved and the composite structure to return to equilibrium; on the other hand, applying vacuum pressure to the jamming structures rapidly dissipates the energy of the projectile and preserves the composite structure in a deformed state.

In addition, it was shown that the impact response of aerial robots can be tuned by constructing landing gear consisting of laminar jamming structures. By applying an appropriate vacuum pressure to the jamming structures (ideally, the lowest possible pressure that still prevents bottoming out), peak forces can be minimized, decay can be accelerated, and shock loads can be mitigated. Thus, jamming-based landing gear has potential to meet the design requirements of aerial vehicles in the robotics literature (e.g., [16], [17]). In addition, since vacuum pressure can rapidly adjust the mechanical properties of jamming structures, the ideal vacuum pressure can be selected right before collision, eliminating the requirement to land at a predetermined speed.

As a third contribution, the present work provides designers with an analytical toolkit for rapidly predicting the dynamic response of laminar jamming structures. In general, jamming structures exhibit highly nonlinear, hysteretic behavior that can be challenging to anticipate; this latter formulated and experimentally validated a dynamic lumped-parameter model that captures the essential features of the dynamic response (i.e., oscillation frequency, oscillation amplitude, and steady-state deformation) and can be simulated in seconds. The only calibration step required is a quasi-static cyclic loading test at the pressures of interest. Furthermore, the model offers an effective method for relating functional requirements to design inputs; for example, if a jamming-based system must exhibit nonzero damping at low force inputs, then F_d should be minimized; as Tables I and II both show, pressure should be reduced, but not relieved entirely. Thus, the models in this latter allow designers to predict the dynamic response of jamming structures with nominal effort, as well as meet specific design goals.
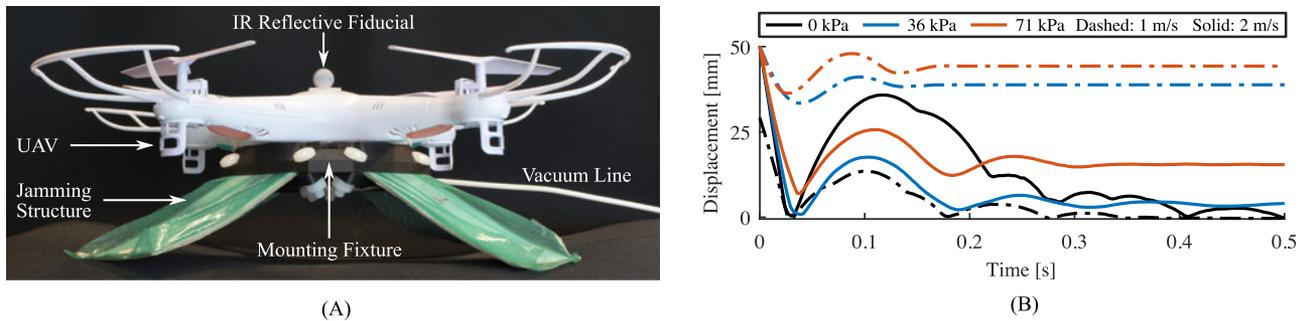
Fig. 7. Tuning the impact response of a traditional rigid robotic system using laminar jamming. (A) UAV with landing gear consisting of four jamming structures. (B) Time response of UAV chassis displacement at two different landing velocities and three different vacuum pressures. Displacement is relative to bottom-out position (i.e., bottom-out = 0 mm). Time is relative to touchdown (i.e., initial contact = 0 s). (Video S2)

Aside from altering impact responses, the capability of laminar jamming structures to tune dynamic responses may have other applications. In fact, the multiple existing methods to actuate jamming structures (e.g., electrostatic [14], elastic[11]) facilitate their integration into diverse systems. For instance, laminar jamming structures may be coupled to dielectric elastomer- and hydrogel-based oscillators [18] to tune their frequency response in real-time, increasing their versatility as acoustic elements and fluidic capacitors. Furthermore, laminar jamming structures may be used as vibration suppression layers in rapidly-actuated soft robots, which are prone to undesired oscillations [19], [20].

IV. CONCLUSION

The present work has demonstrated that laminar jamming structures can effectively tune dynamic responses in real-world robotic systems while overcoming the limitations of existing variable-impedance mechanisms. Furthermore, through analytical and experimental investigations, the latter formulates a lumped-parameter model that can enable designers to rapidly predict the dynamic response of jamming structures and meet specific design requirements. Future work will focus on integrating laminar jamming into additional dynamic systems, as well as building an interactive tool in which designers can determine the optimal dimensions and material properties of a laminar jamming structure given ideal dynamic response characteristics.

ACKNOWLEDGMENT

REFERENCES

[1] B. Vanderborght *et al.*, "Variable impedance actuators: A review," *Robot. Auton. Syst.*, vol. 61, pp. 1601–1614, 2013.

[2] G. Grioli *et al.*, "Variable stiffness actuators: The user's point of view," *Int. J. Robot. Res.*, vol. 34, pp. 727–743, 2015.

[3] M. Cianchetti *et al.*, "Soft robotics technologies to address shortcomings in today's minimally invasive surgery: The STIFF-FLOP approach," *Soft Robot.*, vol. 1, pp. 122–131, 2014.

[4] M. Manti, V. Cacucciolo, and M. Cianchetti, "Stiffening in soft robotics," *IEEE Robot. Autom. Mag.*, vol. 23, no. 3, pp. 93–106, Sep. 2016.

[5] S. Kawamura *et al.*, "Development of passive elements with variable mechanical impedance for wearable robotics," in *Proc. IEEE Int. Conf. Robot. Autom.*, 2002, pp. 248–253.

[6] M. Bureau, T. Keller, R. Velik, J. Perry, and J. Veneman, "Variable stiffness structure for limb attachment," in *Proc. IEEE Int. Conf. Rehabil. Robot.*, 2011, pp. 1–4.

[7] Y. Kim, S. Cheng, S. Kim, and K. Iagnemma, "A novel layer jamming mechanism with tunable stiffness capability for minimally invasive surgery," *IEEE Trans. Robot.*, vol. 29, no. 4, pp. 1031–1042, Aug. 2013.

[8] J. Ou, L. Yao, D. Tauber, J. Steimle, R. Niiyama, and H. Ishii, "JamSheets: Thin interfaces with tunable stiffness enabled by layer jamming," in *Proc. 8th Int. Conf. Tangible Embedded Embodied Interact.*, 2014, pp. 65–72.

[9] T. Simon, B. Thomas, and R. Smith, "Low-profile jamming for medical rehabilitation," *IT Prof.*, vol. 17, pp. 28–34, 2005.

[10] R. Deimel and O. Brock, "A novel type of compliant and underactuated robotic hand for dexterous grasping," *Int. J. Robot. Res.*, vol. 35, pp. 161–185, 2016.

[11] J. Santiago, I. Godage, P. Gonthina, and I. Walker, "Soft robots and kangaroo tails: Modulating compliance in continuum structures through mechanical layer jamming," *Soft Robot.*, vol. 3, pp. 54–63, 2016.

[12] Y. Narang, J. Vlassak, and R. Howe, "Mechanically versatile soft machines through laminar jamming," [In Review].

[13] T. Yokoyama and K. Nakai, "Evaluation of in-plane orthotropic elastic constants of paper and paperboard," in *Proc. Conf. Expo. Exp. Appl. Mech.*, 2007.

[14] M. Henke and G. Gerlach, "On a high-potential variable-stiffness device," *Microsyst. Technol.*, vol. 20, pp. 599–606, 2014.

[15] S. Rao, *Mechanical Vibrations*. Upper Saddle River, NJ, USA: Pearson Prentice Hall, 2004.

[16] S. Dastoor and M. Cutkosky, "Variable impedance due to electromechanical coupling in electroactive polymer actuators," in *Proc. IEEE/RSJ Int. Conf. Intell. Robots Syst.*, 2011, vol. 1, pp. 774–779.

[17] G. Mikulowsky and L. Jankowski, "Adaptive landing gear: Optimum control strategy and potential for improvement," *Shock Vibration*, vol. 16, pp. 175–194, 2009.

[18] C. Keplinger, J.-Y. Sun, C. Foo, P. Rothemund, G. Whitesides, and Z. Suo, "Stretchable, transparent, ionic conductors," *Science*, vol. 341, pp. 984–987, 2013.

[19] B. Mosadegh *et al.*, "Pneumatic networks for soft robotics that actuate rapidly," *Adv. Functional Mater.*, vol. 24, pp. 2163–2170, 2013.

[20] N. Bartlett *et al.*, "A 3d-printed, functionally graded soft robot powered by combustion," *Science*, vol. 10, pp. 161–165, 2015.